Table 1
Biodegradable poly(L-lactide-*co*-ε-caprolactone) (PLCL) copolymer[a]

| Polymer code | Monomer feed ratio | Copolymer composition[b] | Molecular weight[c] | | Physical state at 25 °C |
|---|---|---|---|---|---|
| | LL:CL | LL:CL | Mn | Mw/Mn | |
| PLL | 100:0 | 100:0 | $4.5 \times 10^5$ | 1.3 | Hard solid |
| PLCL 70/30 | 70:30 | 74:26 | $2.0 \times 10^5$ | 1.8 | Hard solid |
| PLCL 50/50 | 50:50 | 50:50 | $2.6 \times 10^5$ | 1.8 | Elastomer |
| PLCL 30/70 | 30:70 | 31:69 | $1.5 \times 10^5$ | 2.2 | Gummy solid |
| PCL | 0:100 | 0:100 | $1.8 \times 10^5$ | 2.1 | Hard solid |

[a]Reaction condition; 150 °C for 24 h under vacuum.
[b]Determined by $^1$H-NMR.
[c]Determined by GPC in chloroform (Polystyrene (PS) standard). Mn: number-average molecular weight, Mw: weight-average molecular weight, polydispersity: Mw/Mn. In PS calibrated GPC measurements, the actual molecular weights of aliphatic polyesters may be overestimated, depending on their structures and molecular weights [20].

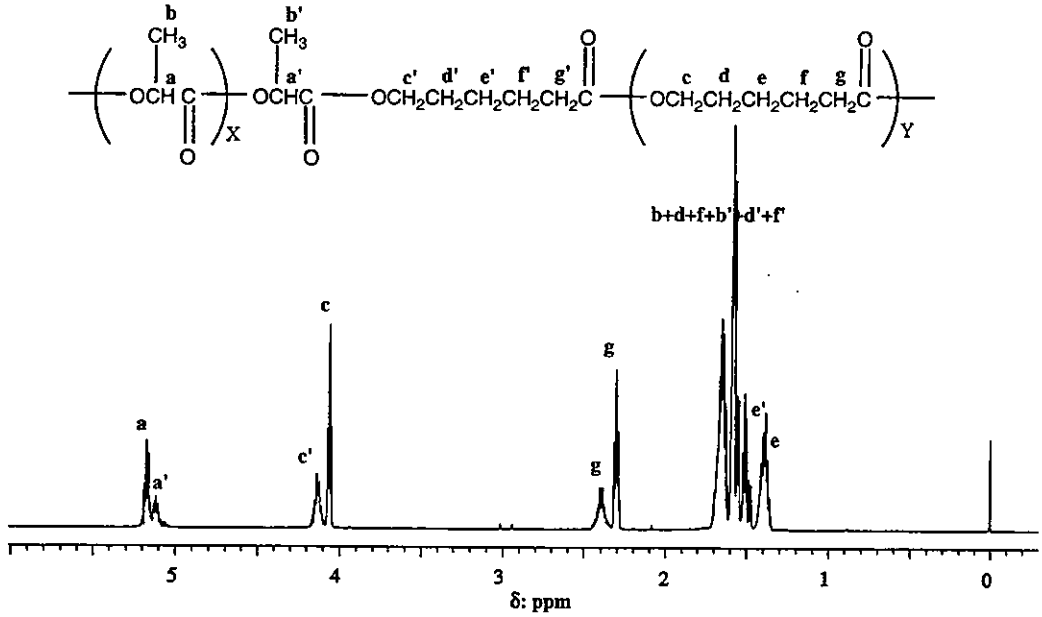


Fig. 1. $^1$H-NMR spectrum and assignment of PLCL 50/50.

number-average molecular weight (Mn) and polydispersity (Mw/Mn) (Mw: the weight-average molecular weight) of the copolymers, determined by GPC, ranged from approximately $1.5 \times 10^5$ to $4.5 \times 10^5$ and 1.3 to 2.2, respectively. The resultant copolymers were solid except for PLCL 30/70 (30 wt% for LL and 70 wt% for CL: the designation of copolymers is given in Table 1), which is gummy.

Microfiber fabrics of good quality with different compositions of PLCL were obtained by electrospinning using MC solution at the predetermined operation conditions (Table 2). All the electrospun fabrics produced consisted of microscale fibers, ranging between approximately 4.3 and 7.0 μm in diameter, except for PLCL 30/70 which produced fused meshes probably due to its inherent physical property (gummy state) (Table 2). PLL microfibers had nanoscale pores approximately 200–800 nm in diameter at the surface and subsurface regions (Fig. 2a), which was also observed by the other research group [21]. On the other hand, such a surface structure was hardly observed for the microfiber fabrics made of the other CL-containing copolymers (Fig. 2b–e). The uniaxial tensile strength measurement test on the electrospun microfiber fabrics showed that the highest tensile strength as well as the highest Young's modulus was observed for the PLL microfiber fabric, followed by PLCL 70/30 (Fig. 3 and Table 2). Both fabrics were torn upon further elongation. PCL exhibited a relatively low Young's modulus but a high creep characteristic. The microfiber fabric

Table 2
Conditions and diameter of PLCL microfiber fabrics[a]

| | Composition LL:CL | Polymer conc. in MC (wt%) | Mean diameter[b] (μm) | Young's modulus[c] (MPa) |
|---|---|---|---|---|
| PLL | 100:0 | 4 | 4.5±0.34 | 17.2 |
| PLCL 70/30 | 74:26 | 9 | 4.3±1.27 | 14.2 |
| PLCL 50/50 | 50:50 | 7 | 7.0±1.03 | 0.8 |
| PLCL 30/70 | 31:69 | 11 | — | — |
| PCL | 0:100 | 7.5 | 5.6±0.61 | 3.6 |

[a]Fixed electrospun conditions: flow rate, 10 ml/h; voltage, 12.5 kV; air gap, 30 cm.
[b]Measured for 20 fibers observed in scanning electron micrographs ($r_{AV}$±SD/μm).
[c]Young's modulus was determined from the slope in the initial linear region of the stress–strain curves of the fabrics of thickness of approximately 140 μm.

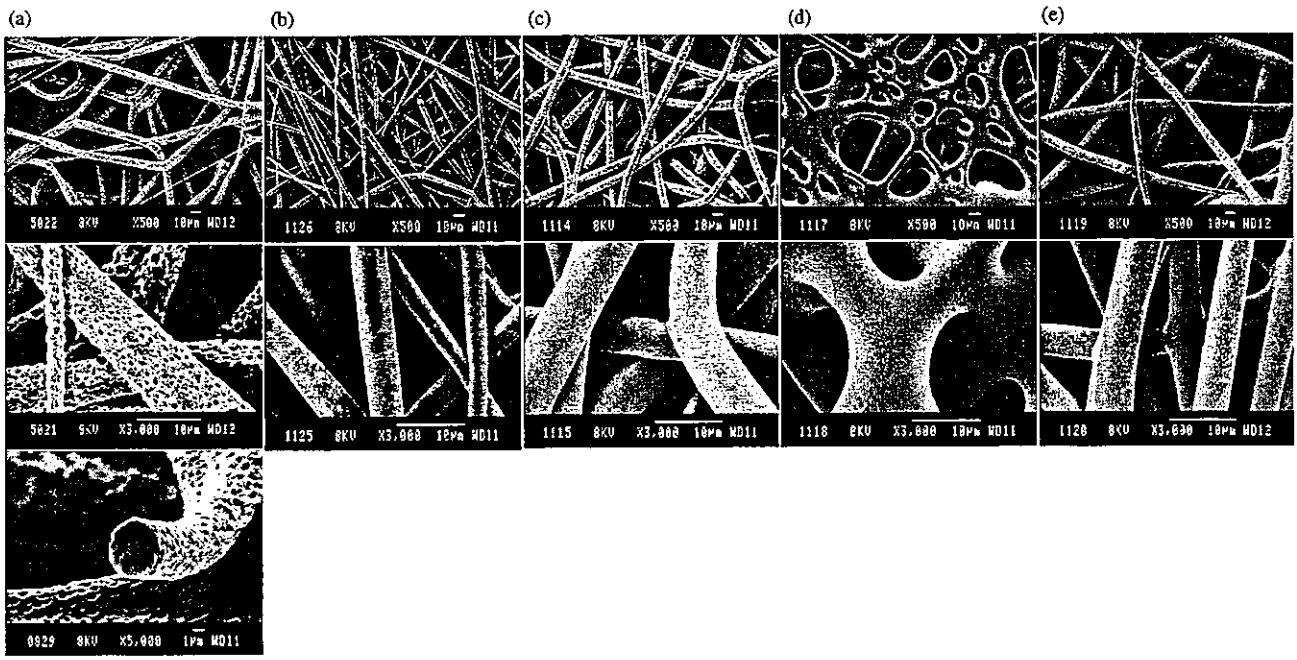


Fig. 2. SEM images of electrospun microfiber fabrics made of PLCL (co)polymers: (a) PLL, (b) PLCL 70/30, (c) PLCL 50/50, (d) PLCL 30/70, and (e) PCL.

made of PLCL 50/50 was elastomeric as shown by a low Young's modulus and an almost linear stress–strain relationship under the maximal stain (500%) in this measurement (Fig. 3 and Table 2).

### 3.2. Electrospun PLCL 50/50 nano- to microfiber fabrics

The mechanical strength and porosity of fabric depend on fiber composition, fiber diameter and fabric density. Nano- to microfiber fabrics were prepared using the equimolar copolymer PLCL 50/50 using different solvents under different operation conditions. This eliminates the polymer composition effect on the mechanical property and porosity of the fabrics. Table 3 shows the electrospinning conditions for the nano- to microfiber fabrics made of the copolymer. Nanoscale-fiber fabric (0.32±0.08 μm; designated fabric A) was electrospun at a concentration of 3 wt% in HFIP under a high voltage (30 kV) and a low flow rate (5 ml/h), whereas a fabric of almost 1-μm diameter fiber (1.16±0.17 μm, fabric B) was obtained at a low voltage (15 kV) and a high flow rate (10 ml/h). As described above, a fiber fabric of more than several microns in diameter (7.02±1.03 μm, fabric C) was obtained using MC solvent (Table 3). Fig. 4 shows the cross-sectional SEM images of these fabrics with a thickness of approximately 140 μm. A highly interconnected porous structure was observed, irrespective of fiber diameter.

The porosities of these fabrics with different fiber diameters were determined using a mercury intrusion

porosimeter. Fig. 5 shows the differential intrusion volume vs. pore diameter relationship on the electrospun fabrics with approximately the same thickness (140 μm), indicating that multiple peak profiles in the pore diameter ranging between ca. 0.2 and 400 μm. Regarding pore distribution, most of the pore volumes were observed in the ranges from approximately 0.2 to 30 μm (approximate mean pore diameter of 5 μm) for fabric approximately 0.2–400 μm (two peaks; approximate mean pore diameter of 80 and 40 μm) for fabric B, and approximately 1–500 μm (approximate mean pore diameter of 50 μm) for fabric C. As shown in Table 4, the calculated porosities ($P_C$), determined from the density of the fabrics and the density of copolymer according to the equation in the footnote of Table 4, were much higher than the porosities determined by the mercury intrusion porosimeter method. The lowest total pore volume ($V_P$; ml/g) and porosity ($P_M$), both of which were determined by the mercury intrusion porosimeter measurement, were found for fabric A. There were small significant differences in $V_P$ and $P_M$ between fabrics B and C, despite the fact that the density of fabric C was higher than that of fabric B.

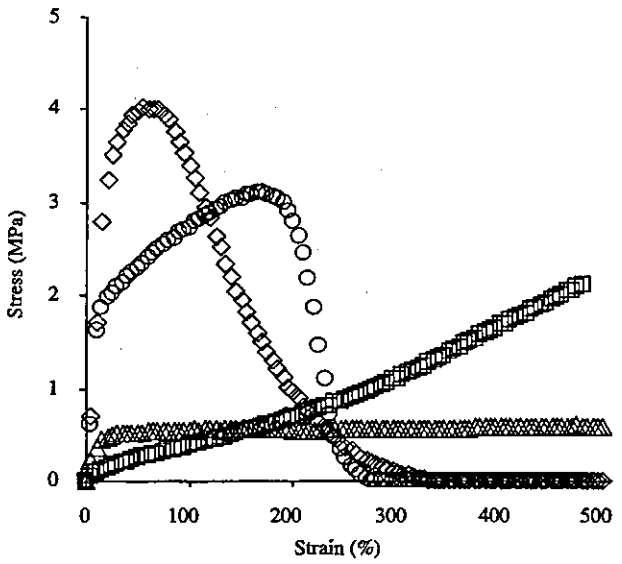


Fig. 3. Stress–strain curves for electrospun microfiber fabrics made of PLCL (co)polymers: PLL (◇), PLCL 70/30 (○), PLCL 50/50 (□), and PCL (△). Mean for $n = 4$.

Fig. 6 shows the stress–strain relationships of these nano- to microfiber fabric sheets with a thickness of approximately 140 μm (a solvent-cast film was included in comparison). Irrespective of fiber diameter, a fairly linear relationship was obtained even at 500% of strain, whereas the solvent-cast film showed a very steep linear relationship at a very low strain, followed by a creep characteristic. Young's modulus increased with a decrease in the fiber diameter of the fabric (Fig. 6 and Table 3).

### 3.3. Cell adhesion and proliferation potentials

The adhesion, spreading and proliferation potentials of HUVECs on fabrics made of fibers of different diameters (A, B and C in Table 3) were evaluated for 1, 4, and 7 days after seeding the cells. Cells highly elongated on fibrous meshes were observed for the fabrics made of 0.3-μm-diameter fibers (A) and 1.2-μm-diameter fibers (B) (Fig. 7). However, round or restricted-spread cells were observed on the fibers, which were quite sparsely distributed on the surface of fabric C made of 7 μm-diameter fibers. The densities of cells on the fabrics increased with incubation time for both fabrics (A and B), whereas a very low density of adhering cells on fabric C remained without any sign of proliferation even at 1-week culture (Fig. 8).

## 4. Discussion

The design and fabrication of scaffolds are an essential task for a functional vital engineered tissue. A provisional scaffold serves as a temporal cell adhesion and proliferation bed until natural ECM is generated by

Table 3
Electrospun PLCL 50/50 fabrics

| Code name | Solvent | Polymer conc. (wt%) | Flow rate (ml/h) | Voltage (kV) | Air gap (cm) | Mean diameter[c] (μm) | Young's modulus[d] (MPa) |
|---|---|---|---|---|---|---|---|
| A | HFIP[a] | 3 | 5 | 30 | 20 | 0.32±0.08 | 2.2 |
| B | HFIP | 3 | 10 | 15 | 20 | 1.16±0.17 | 1.8 |
| C | MC[b] | 7 | 10 | 13 | 30 | 7.02±1.03 | 0.8 |

[a]1,1,1,3,3,3-Hexafluoro-2-propanol (boiling point, 58 °C; dielectric constant and surface tension, 17.8 and 16.14 dyn/cm, respectively at 25 °C). (CAS No.920-66-1) [22].

[b]Methylene chloride (MC) (boiling point, 39 °C; dielectric constant and surface tension, 8.93 and 27.1 dyn/cm, respectively at 25 °C). [CAS No.75-09-2].

[c]Measured for 20 fibers observed in scanning electron micrographs ($R_{AV}$±SD/μm).

[d]Young's modulus was determined from the slope in the initial linear region of the stress–strain curve of the film of thickness of approximately 140 μm.

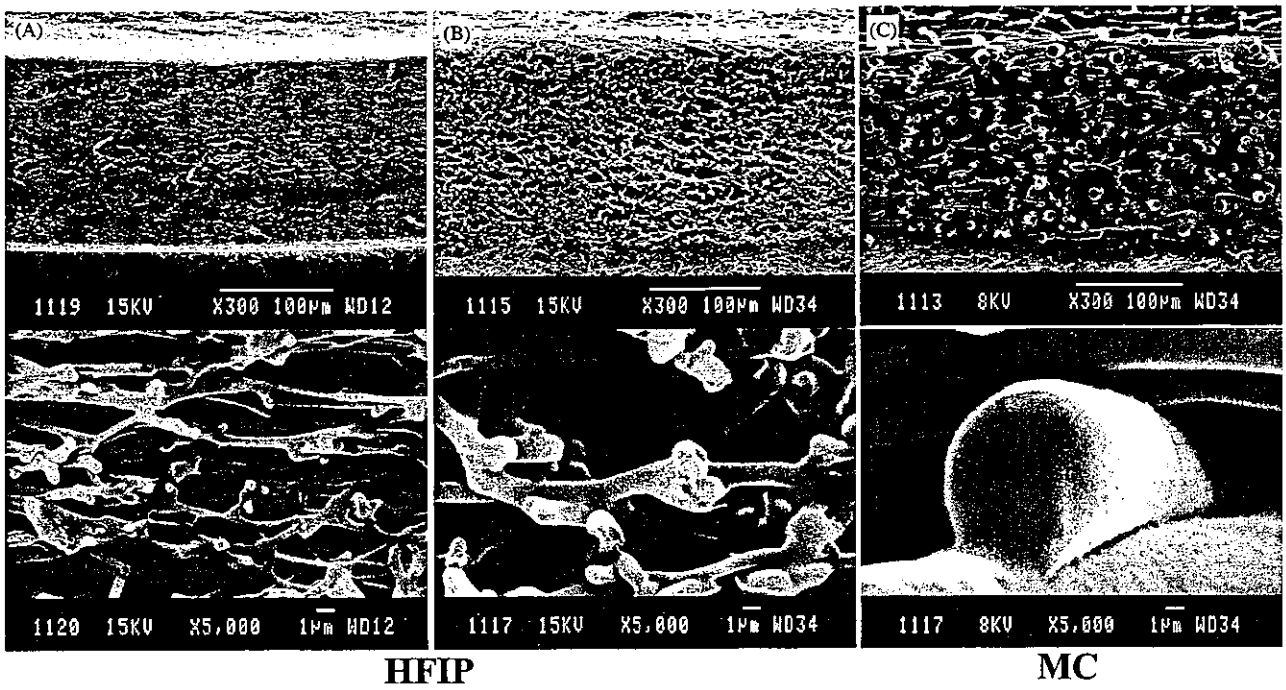


Fig. 4. SEM images of electrospun nano- to microfiber fabrics made of PLCL 50/50 copolymer. Mean diameters of fibers: (A) 0.3 μm, (B) 1.2 μm, and (C) 7 μm.

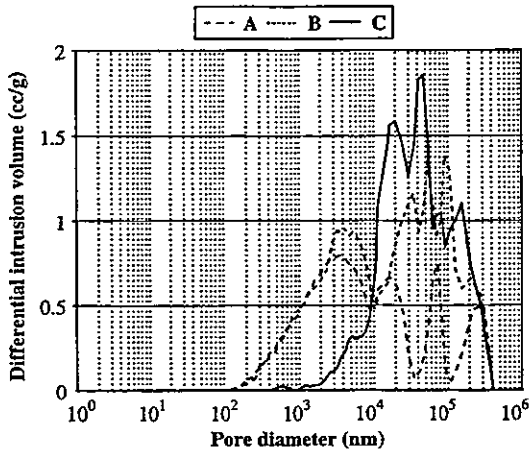


Fig. 5. Representative plots of differential intrusion volume vs. pore diameter of electrospun nano- to microfiber PLCL 50/50 fabrics. Mean diameters of fibers: (A) 0.3 μm, (B) 1.2 μm, and (C) 7 μm.

inoculated cells to form a tissue morphology resembling that of a native tissue. ECM consists of a nanoscale fibrous network of proteins and proteoglycans. Such topographical cues may have significant effects on cell behavior. To fabricate a provisional biomimetic scaffold composed of nano- to microscale fibrous meshes, electrospinning has been proven to be an effective method [11,12]. In addition to the topographical feature of a scaffold, the mechanical properties of a scaffold are another important aspect, which can be regulated by the material itself and the design of the structure. That is, a designed scaffold should not only be to provide a surface for cell residence but also to maintain sufficient biomechanical support during tissue regeneration and structure degradation. For provisional nano- or microscale fibrous meshes, biodegradable and bioabsorbable (co)poly(ester)s have been extensively studied [1,6–9]. However, a systematic study focusing on the effects of the copolymer composition and mean fiber diameter of electrospun fibrous meshes on the mechanical properties, cell adhesion and proliferation potentials has not been carried out yet.

In this study, electrospun microfiber fabrics made of a series of PLCLs with different compositions were prepared from their MC solutions. Interestingly, only PLL, which tends to exhibit a partially crystalline structure, produced nanoscale pores along the electrospun fiber surface (Fig. 2a). This phenomenon was in accordance with the experimental evidence reported by Bognitzki et al. who rationalized that the rapid phase separation induced by the evaporation of the solvent and the subsequent rapid solidification during electrospinning may be accounted for this structured surface [21]. Such nanoporous surface structuring was not observed on electrospun PLCLs and PCL microfabrics (Fig. 2b–e) [16]. Among the (co)polyesters with graded compositions (Table 1), only the equimolar copolymer PLCL 50/50 exhibited an elastomeric behavior (Fig. 3).

Table 4
Porosimetry of electrospun nano- to microfiber PLCL 50/50 fabrics[f]

| Code name (mean fiber diameter) | Sample weight $W$/g | Sample volume $V$/cm$^3$ | Density[a] $D$/ g cm$^{-3}$ | Calculated porosity[b] $P_C$/% | Porosimetry[c] | |
|---|---|---|---|---|---|---|
| | | | | | Total pore volume[d] $V_P$/ml g$^{-1}$ | Porosity[e] $P_M$/% |
| A (0.3 μm) | 0.0503 | 0.134 | 0.375 | 69 | 1.49 | 56 |
| B (1.2 μm) | 0.0399 | 0.140 | 0.285 | 76 | 2.29 | 61 |
| C (7.0 μm) | 0.0415 | 0.133 | 0.313 | 74 | 2.01 | 63 |

[a] $D$: weight/volume.
[b] Calculated porosity: $P_C = (1-d_m/d_p) \times 100$ ($d_m$: density of mesh, $d_p$: density of PLCL 50/50 = 1.21 g/cm$^3$).
[c] Measured by a mercury intrusion porosimeter.
[d] $V_P$: total mercury intrusion volume.
[e] Measured porosity: $P_M = V_P W$ 100/V.
[f] Thickness: approximately 140 μm.

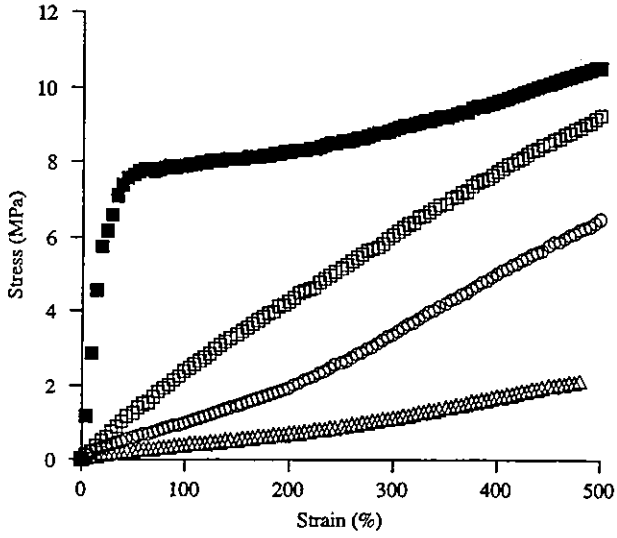


Fig. 6. Stress–strain curves for electrospun nano- to microfiber PLCL 50/50 fabrics. Mean diameter: 0.3 μm (□), 1.2 μm (○), 7 μm (△), and solvent-cast film (■). Mean for $n = 4$.

The fiber diameter of fabric made of PLCL 50/50 was controlled by the type of solvent used and operation parameters (Fig. 4: A, B, and C). As tabulated in Table 3, nanofiber fabric A, which was electrospun using HFIP (boiling point, 59 °C; dielectric constant, 17.8; and surface tension, 16.14 dyn/cm at 25 °C) as a solvent at a high applied voltage (30 kV) and a low flow rate (5 ml/h), produced a very fine fiber network (mean fiber diameter, 0.3 μm), whereas the fiber diameter produced with the same solution increased at a low applied voltage (15 kV) and a high flow rate (10 ml/h) (B: 1.2 μm). On the other hand, a microfiber fabric (C: 7.0 μm) was produced using MC (boiling point, 39 °C; dielectric constant, 8.9; and surface tension, 27.1 dyn/cm at 25 °C) using different operation parameters. Theoretically, a small fiber diameter should be obtained using a solvent having a low surface tension and a high dielectric constant under the operation conditions of a high applied voltage and a low flow rate [23]. That is, nanofibers are formed by the narrowing of the ejected jet stream as it undergoes increasing surface charge density due to evaporation of the solvent. Finer jet stream is generated by very strong electrostatic repulsion of a charged fiber surface during flight of a jet stream and subsequent burst, resulting in the formation of instable jet streams. Although the authors did not conduct a systematic approach to regulate fiber diameter, our data (Table 3) appear to follow the theoretical prediction.

As shown in Table 4 and Fig. 5, the difference in fiber diameter among the electrospun fabrics led to differences in specific density (or degree of packing of fibers), mean pore diameter and pore distribution among the fabrics. The densest fabric was found to be fabric A with the smallest fiber diameter. Both porosities (calculated and experimentally obtained), total pore volume, and mean pore diameter (approximately 5 μm; Fig. 5) were also lowest among the three fabrics (see Table 4). On the other hand, the medium-sized-fiber fabric B and large-sized-fiber fabric C had almost the same porosities (regardless of calculated or experimentally obtained one), total pore volumes and densities although the differences in mean fiber diameter were quite large (1.2 μm for B and 7.0 μm for C). Porosity can be expressed as

$$P = 1 - d_m/d_p, \tag{1}$$

which can be rewritten as

$$P = 1 - \pi r^2 L/V \tag{2}$$

since the following relation holds

$$d_m = \pi r^2 L d_p/V. \tag{3}$$

In these equations, $P$ is porosity of fabric, $d_m$ and $d_p$ are densities of mesh and polymer, respectively, $r$ is mean

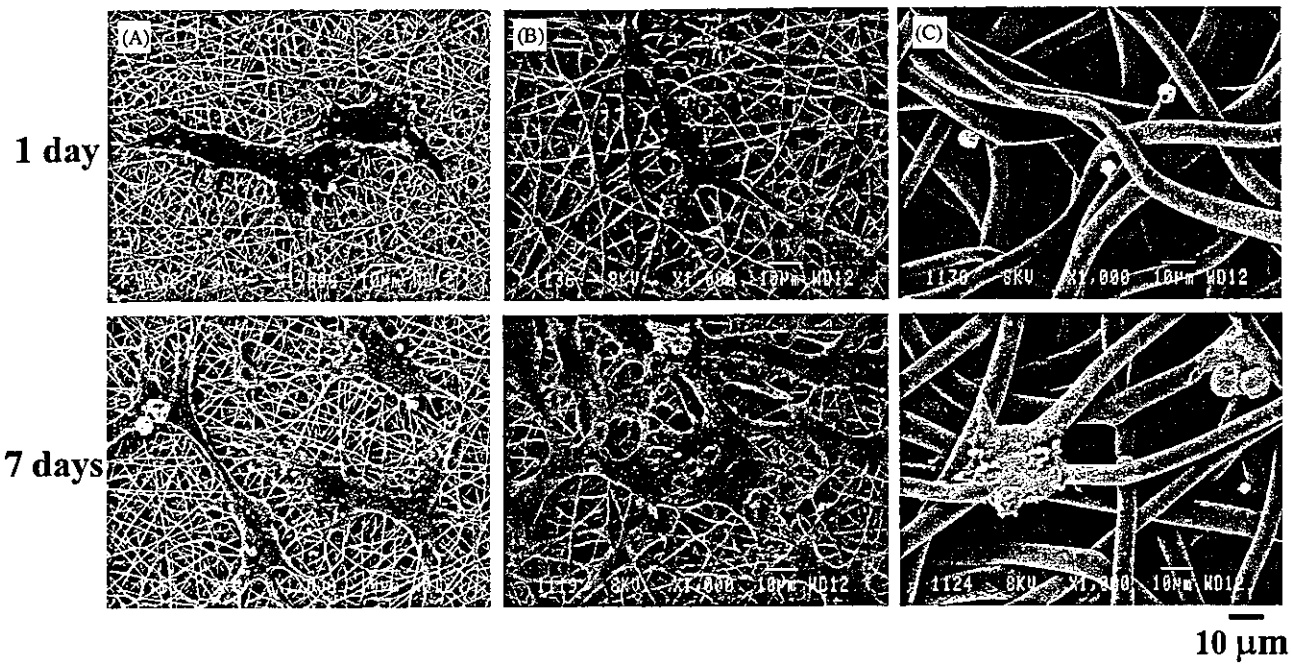


Fig. 7. SEM images of cells (HUVECs) cultured for 1 and 7 days on electrospun PLCL 50/50 fabrics with different-diameter fibers: (A) 0.3 μm, (B) 1.2 μm, and (C) 7 μm.

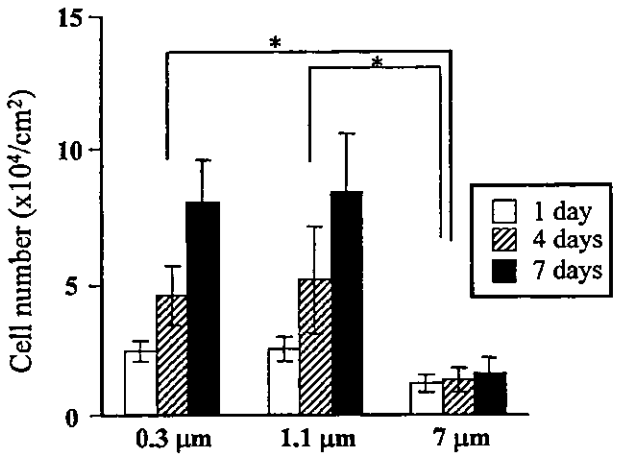


Fig. 8. Time-dependent number of cells (HUVECs) adhered on electrospun PLCL 50/50 fabrics with different-diameter fibers. Mean for $n = 4 \pm$ SD ($p < 0.05$).

radius of fiber and $L/V$ is total fiber length ($L$) in the unit volume ($V$). Eq. (2) describes that $r$ and $L/V$ independently affect $P$. Therefore, under the condition of almost the same porosity, the exponential decrease in the fiber diameter must result in the linear increase of fiber density of fabric. This is qualitatively visualized by SEM (Fig. 4). On the other hand, the pore size distribution greatly depended on the mean fiber diameter (Fig. 5): a very high population of smaller-pore region (0.1–10 μm) and a low population of medium- to large-sized-pore region (10–400 μm) were observed for the highest dense fabric A, whereas the least dense fabric C had few small-sized pores but many large-sized pores. The intermediately dense fabric B exhibited a biphasic pore-distribution characteristic of these two high and low fiber density-fabrics.

The mechanical properties of non-woven fabrics depend on geometrical structures of fibers [24]. The highest Young's modulus was observed for highest dense fabric A, followed by that of fabric B and the lowest Young's modulus was observed for least dense fabric C at almost the same porosity or density (Fig. 6 and Table 3). This indicates that a decrease in the fiber diameter of fabric increases mechanical strength probably due to the increase of the fiber density.

As for the behavior of cells on the fabrics, the higher cell adhesion and proliferation potential of HUVECs were noted on both the small- and medium-sized-fiber fabrics (A and B) compared with fabric C (Figs. 7 and 8). The numbers of fibers existing at the unit area of outermost surfaces of the fabrics, determined from the SEM images (40 μm × 40 μm; $n = 4$), were as follows: $40.5 \pm 4.5/1600\ \mu m^2$ for fabric A, $15.1 \pm 2.2/1600\ \mu m^2$ for fabric B and $2.5 \pm 0.6/1600\ \mu m^2$ for fabric C. The surface of the dense fabric eventually enabled the adhesion, spreading and proliferation of cells which anchored on many fibers at the outermost surface, as observed in fabrics (A and B) (Figs. 7 and 8). On the other hand, the most sparsely distributed fabric with the largest

diameter (fabric C) provided quite different types of cell behavior: cells adhered on a single fiber are round-shaped and non-proliferating cells predominated. Such behaviors should result from a large interfiber distance or a very low surface density of fibers, which did not permit cell adhesion across the neighboring fibers.

There has been an increasing interest in nanoscale fibrous synthetic scaffolds associated with the biomimicking of the basement membrane which shows a nano- to submicron-scale topography of extracellular matrix macromolecules, including fiber meshes [6–9], pores [25], ridges [26], grooves [26], and peak valleys [27]. Among nanoscale biodegradable synthetic polymers, (co)poly(ester)s such as PLL, poly(lactide-*co*-glycolide) (PLGA), PCL and PLCL have been fabricated into nanofibers by electrospinning [6–9,21]. Cell adhesiveness and proliferability on these fabrics were reported, and the potential applications for tissue engineering based upon its unique architecture, which serves to support and guide cell growth were discussed [6–9]. Highly packed fabrics or high-surface-density fibers provide an extremely high surface-to-volume ratio, which favors cell attachment and proliferation [8]. The results of our present study agreed very well with those of previous studies. Taken together with the results obtained in this study, a more functional biodegradable polymer-based "bioactive" and "mechano-active" tubular scaffold for vascular tissue replacement technology will be reported in the near future.

## 5. Conclusion

Highly interconnected porous nano- to microfiber fabrics made of PLCL copolymers with different compositions were electrospun. Different fabric architectures of the elastomeric copolyester, the equimolar PLCL copolymer, were prepared using different solvents. The decrease in the fiber diameter of fabric resulted in a decrease in porosity and pore size, but an increase in fiber density and mechanical strength. HUVECs were well adhered and proliferated on the highly packed nano- and 1-micron-scaled-fiber fabrics. The discussion suggests that electrospun elastomeric nanofiber fabric thus prepared may be useful as provisional functional scaffolds in cardiovascular and muscular tissue engineerings.

## Acknowledgements

The authors thank Dr. T. Kanemaru of the Faculty of Medicine, Kyushu University, for SEM. This study was financially supported in part by a Grant-in-Aid for Scientific Research (A2-15200038) from Ministry of Education, Culture, Sports, Science, and Technology (MEXT), Japan.

## References

[1] Mikos AG, Bao Y, Cima LG, Ingber DE, Vacanti JP, Langer R. Preparation of PGA bonded fibre structure for cell attachment and transplantation. J Biomed Mater Res 1993;27:183–9.
[2] Park A, Wu B, Griffith LG. Integration of surface modification and 3D fabrication techniques to prepare patterned poly (L-lactide) substrates allowing regionally selective cell adhesion. J Biomater Sci Polym Ed 1998;9:89–110.
[3] Kwon IK, Park KD, Choi SW, Lee SH, Lee EB, Na JS, Kim SH, Kim YH. Fibroblast culture on surface-modified poly(glycolide-*co*-ε-caprolactone) scaffold for soft tissue regeneration. J Biomater Sci Polym Ed 2001;12:1147–60.
[4] Elsdale T, Bard J. Collagen substrata for studies on cell behavior. J Cell Biol 1972;54:626–37.
[5] Curtis ASG, Riehle MO. Tissue engineering: the biophysical background. Phys Med Biol 2001;46:47–65.
[6] Li WJ, Laurencin CT, Caterson EJ, Tuan RS, Ko FK. Electrospun nanofibrous structure: a novel scaffold for tissue engineering. J Biomed Mater Res 2002;60:613–21.
[7] Yoshimoto H, Shin YM, Terai H, Vacanti JP. A biodegradable nanofibers scaffold by electrospinning and its potential for bone tissue engineering. Biomaterials 2003;24:2077–82.
[8] Mo XM, Xu CY, Kotaki M, Ramakrishna S. ElectrlspunP(LLA-CL) nanofiber: a biomimetic extracellular matrix for smooth muscle cell and endothelial cell proliferation. Biomaterials 2004;25:1883–90.
[9] Reneker DH, Kataphinan W, Theron A, Zussman E, Yarin AL. Nanofiber garlands of polycaprolactone by electrospinning. Polymer 2002;43:6785–94.
[10] Matthews JA, Wnek GE, Simpson DG, Bowlin GL. Electrospinning of collagen nanofibers. Biomacromolecules 2002;3:232–8.
[11] Reneker DH, Chun I. Nanometre diameter fibres of polymer, produced by electrospinning. Nanotechnology 1996;7:216–23.
[12] Shin YM, Hohman MM, Brenner MP, Rutledge GC. Experimental characterization of electrospinning: the electrically forced jet and instabilities. Polymer 2001;42:9955–67.
[13] de Groot JH, Zijlstra FM, Kuipers HW, Pennings AJ, Klompmaker J, Veth RP, Jansen HW. Meniscal tissue regeneration in porous 50/50 copoly(L-lactide/epsilon-caprolactone) implants. Biomaterials 1997;18:613–22.
[14] den Dunnen WF, van der Lei B, Robinson PH, Holwerda A, Pennings AJ, Schakenraad JM. Biological performance of a degradable poly(lactic acid-epsilon-caprolactone) nerve guide: influence of tube dimensions. J Biomed Mater Res 1995;29:757–66.
[15] Kricheldorf HR, Kreiser-Saunders I, Boettcher C. Polylactones: 31. Sn(II)octoate-initiated polymerization of L-lactide: a mechanistic study. Polymer 1995;36:1253–9.
[16] Hiljanen-Vainio M, Karjalainen T, Seppälä J. Biodegradable lactone copolymers I. Characterization and mechanical behavior of ε-caprolactone and lactide copolymer. J Appl Polym Sci 1996;59:1271–88.
[17] Grijpma DW, Zondervan GJ, Pennings AJ. High molecular weight copolymers of L-lactide and ε-caprolactone as biodegradable elastomeric implant material. Polym Bull 1991;25:327–34.
[18] Kidoaki S, Kwon IK, Matsuda T. Mesoscopic spatial designs of nano- and microfiber meshes for tissue-engineering matrix and scaffold based on newly devised multilayering and mixing electrospinning techniques. Biomaterials 2005;26:37–46.

[19] Washburn EW. Note on a method of determining the distribution of pore sizes in a porous material. Proc Natl Acad Sci USA 1921;7:115–6.
[20] Pasch H, Rode K. Use of matrix-assisted laser desorption/ionization mass spectrometry for molar mass-sensitive detection in liquid chromatography of polymers. J Chromatography A 1995;699:21–9.
[21] Bognitzki M, Czado W, Frese T. Nanostructured fibers via electrospinning. Adv Mater 2001;13:70–2.
[22] Fioroni M, Burger K, Mark AE, Roccatano D. Model of 1,1,1,3,3,3-Hexafluoro-propan-2-ol for molecular dynamics simulations. J Phys Chem B 2001;105:10967–75.
[23] Ma PX, Choi JW. Biodegradable polymer scaffolds with well-defined interconnected spherical pore network. Tissue Eng 2001;7: 23–33.
[24] Lee KH, Kim HY, La YM, Lee DR, Sung NH. Influence of a mixing solvent with tetrahydrofuran and *N,N*-dimethylformamide on electrospun poly(vinyl chloride) Nonwoven mats. J Polym Sci Part B: Polym Phys 2002;40: 2259–68.
[25] Campbell CE, von Recum AF. Microtopography and soft tissue response. J Invest Surg 1989;2:51–74.
[26] den Braber ET, de Ruijter JE, Smits HTJ, Ginsel LA, von Recum AF, Jansen JA. Quantitative analysis of fibroblast morphology on microgrooved surfaces with various groove and ridge dimensions. Biomaterials 1996;17:2037–44.
[27] Dalby MJ, Riehle MO, Johnstone H, Affrossman S, Curtis ASG. In vitro reaction of endothelial cells to polymer demixed nanotopography. Biomaterials 2002;23:2945–54.

ACADEMIC PRESS

Available online at www.sciencedirect.com

SCIENCE DIRECT®

Bioorganic Chemistry 31 (2003) 163–171

BIOORGANIC CHEMISTRY

www.elsevier.com/locate/bioorg

# Polysaccharide–polynucleotide complexes (15): thermal stability of schizophyllan (SPG)/poly(C) triple strands is controllable by α-amino acid modification

Munenori Numata,[a] Takahiro Matsumoto,[a] Mariko Umeda,[a] Kazuya Koumoto,[b] Kazuo Sakurai,[b] and Seiji Shinkai[a,*]

[a] *Department of Chemistry and Biochemistry, Graduate School of Engineering, Kyushu University, 6-10-1 Hakozaki, Higashi-ku, Fukuoka, Fukuoka 812-8581, Japan*

[b] *Department of Chemical Processes and Environments, Faculty of Environmental Engineering, The University of Kitakyushu, 1-1 Hibikino, Wakamatsu-ku, Kitakyushu, Fukuoka 808-0135, Japan*

Received 9 September 2002

**Abstract**

Schizophyllan (SPG), a β-1,3-glucan polysaccharide which is known to form macromolecular complexes with certain polynucleotides, was modified by a reductive amination method with α-amino acids (Arg, Lys, and Ser). The thermal stability of the complexes as estimated by $T_m$ was enhanced in SPG–Arg and SPG–Lys conjugates which have p*I* values higher than the pH of the medium (8.0). The $T_m$ shift increased with the increase in the percentage of α-amino acid introduced and the highest $T_m$ values attained were 64 °C for SPG–Arg conjugate and 62 °C for SPG–Lys conjugate, which are higher by 13 and 11 °C, respectively, than those of the unmodified SPG + poly(C) complex. In the SPG–Ser conjugate with a p*I* lower than the medium pH (8.0), the $T_m$ values decreased with an increase in the percentage of Ser. Formation of the macromolecular complex was no longer detected above 13.2% Ser. The findings indicate that the $T_m$ values are easily controllable by the type and percentage of the introduced α-amino acids. We believe, therefore, that the present conjugates, consisting of naturally originated SPG and α-amino acids, provide an important lead for developing nontoxic artificial vectors and to control the affinity with polynucleotides in response to medium pH and temperature.


* Corresponding author. Fax: +81-92-642-3611.
*E-mail address:* seijitcm@mbox.nc.kyushu-u.ac.jp (S. Shinkai).

0045-2068/03/$ - see front matter 
doi:10.1016/S0045-2068(03)00020-8

## 1. Introduction

Schizophyllan (SPG) is a natural polysaccharide produced by the fungus *Schizophyllum commune* and its repeating unit consists of three β-(1 → 3) glucoses and one β-(1 → 6) glucose side-chain linked at every third main-chain glucose (Fig. 1) [1,2]. SPG forms a triple helix in water and dissociates into a single chain (s-SPG) in dimethylsulfoxide (DMSO) [3–5]. The s-SPG chain can regain the original triple helix structure by exchanging DMSO for water [5–7]. Recently, we found that when this solvent-exchange process is carried out in the presence of polynucleotides, the resultant triple helix consists of two s-SPG chains and one nucleotide chain, indicating that the SPG–polynucleotide interaction is energetically more favored than the SPG–SPG interaction under some specific conditions [8,9]. Subsequent study revealed that this complexation is characteristic of water-soluble β-1,3-glucans and not observed for other polysaccharides [10]. As far as we know, this is the first clear evidence that a neutral polysaccharide can form a macromolecular complex with polynucleotides. We believe that s-SPG/polynucleotide complexes may provide a new methodology for gene technology, such as gene carriers, affinity separation columns, biosensors, etc. [11]. In view of these applications, it would be advantageous to be able to control the thermal stability of the complexes by chemical modification of SPG. In this paper, we introduced an amino group into the side-chain of SPG by combining periodate oxidation with subsequent reductive amination (Scheme 1).

To enhance the affinity between SPG and polynucleotides, it seemed most effective and expeditious to introduce cationic groups into either the main-chain or the side-chain glucose units. It is known, however, that selective modification of OH groups in sugar derivatives is fairly difficult. Previously, we found one convenient method, by which one can introduce functional groups only into the side-chain glucose units. This method involves oxidation cleavage by periodate anion ($IO_4^-$) of the 1,2-diol group [12], which in SPG exists only in the side-chain glucose units. Thus, one can "selectively" oxidize the 1,2-diol groups into aldehyde groups, which are useful to introduce various functional groups (Scheme 1). We thus introduced 2-aminoethanol into these aldehyde groups by Schiff base formation followed by $NaBH_4$ reduction [13]. As expected, introduction of only 2.4% of the 2-aminoethanol group (per single side-chain glucose unit) significantly improved the thermal stability of the complex. Compared with the melting temperature of the complex ($T_m$), the 2-aminoethanol-modified SPG + poly(C) complex had a $T_m$ value higher by 8 °C than the unmodified SPG + poly(C) complex [13].

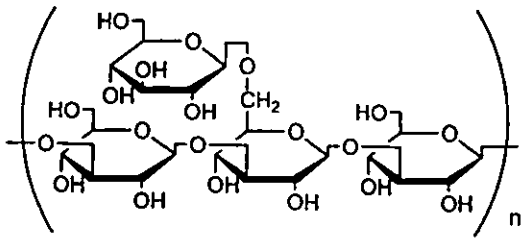


Fig. 1. Repeating unit of schizophyllan [1–4].

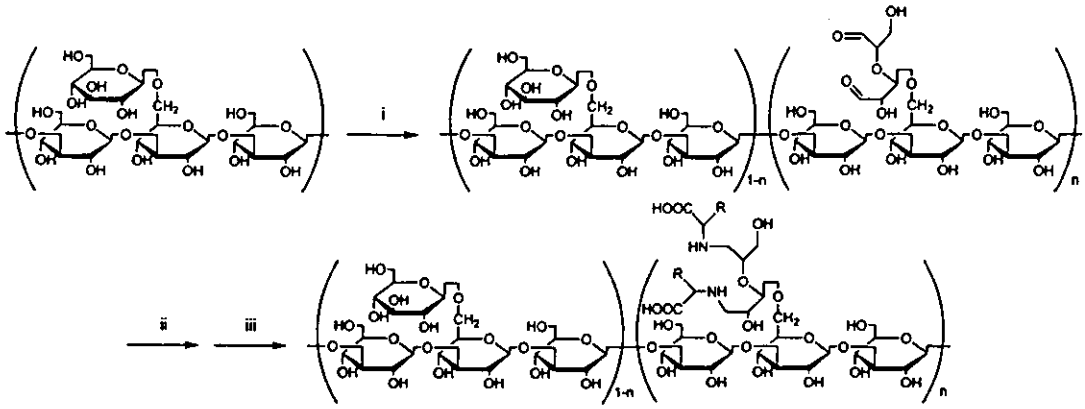

Scheme 1. Schematic illustration for the introduction of α-amino acid groups into SPG: n indicates α-amino acid modification percentage. Reagents and conditions: (i) $NaIO_4$, $H_2O$, 4 °C, 2 days, (ii) α-amino acid methyl ester, $K_2CO_3$, DMSO, r.t., 2 days, (iii) $NaBH_4$, DMSO, r.t., 1 day.

When considering the application of modified SPGs as candidates for artificial vectors, one should introduce, instead of the 2-aminoethanol group, some nontoxic functional group. α-Amino acids satisfy these prerequisites, because they are natural compounds, and have an amino group amenable to the modification method shown in Scheme 1. Furthermore, one can obtain insight into the charge effect of introduced cationic arginine (p$I$ = 10.76), lysine (p$I$ = 9.74), or anionic serine (p$I$ = 5.68) on the thermal stability of the complexes [14]. In this paper, we report not only this charge effect, but also the effect of the percentage of α -amino acid introduced on the thermal stability of the complexes with poly(C).

## 2. Experimental procedure

### 2.1. Materials

SPG was kindly supplied by Taito, Japan. The molecular weight and the number of repeating units were evaluated to be $1.5 \times 10^5$ and 231, respectively [8]. Poly(C) was purchased from Pharmacia, RNase-free distilled water was obtained from Nippon Gene, and spectroscopic grade DMSO was obtained from Kishida and used for all measurements. L-Arginine methyl ester dihydrochloride, L-lysine methyl ester dihydrochloride, and L-serine methyl ester hydrochloride were purchased from Watanabe Chemical Industries.

### 2.2. Methods

The selective oxidation of the 1,2-diol group was carried out as described [13]. The modification ratios of the aldehyde groups introduced were controlled by the amount of sodium periodate ($NaIO_4$). After freezing-and-pumping followed by dialysis (fractionated molecular weight = 12,000; Viskase Companies), SPG with the

aldehyde side-chain was obtained. The general procedure for introduction of α-amino acid to SPG was as follows. $K_2CO_3$ (1.0 g) and oxidized SPG (0.1 g; 0.030 mmol/calculated aldehyde units) were mixed in dry DMSO. To the DMSO solution were added α-amino acid methyl ester hydrochloride (3.0 mmol) and the resultant DMSO mixture was stirred under nitrogen at room temperature. After 2 days, an excess of $NaBH_4$ (0.3 g) was added and the mixture was stirred another 1 day. After quenching unreacted $NaBH_4$ with acetic acid, DMSO and inorganic materials were removed by dialysis under basic conditions. The ester group of the α-amino acid introduced was hydrolyzed to the corresponding acid during this process, because the ester IR peak at 1747 $cm^{-1}$ (nujol) completely disappeared. Freezing-and-pumping of the resulting solution gave the α-amino acid-modified SPG.

The percentage of α-amino acid introduced was determined by elemental analysis. The s-SPG-amino acid/poly(C) complex was prepared by mixing s-SPG-amino acid in DMSO and poly(C) in water, as described [9]. The thermal stability of the complexes was estimated by the CD spectral method, using a J-720WI spectropolarimeter with a 1.0 cm cell.

## 3. Results and discussion

As summarized in Table 1, α-amino acid-modified SPG derivatives were obtained containing 3.6–36.0% Arg [abbreviated as SPG–Arg(3.6)–SPG–Arg(36.0)], 6.6–31.7% Lys [abbreviated as SPG–Lys(6.6)–SPG–Lys(31.7)], and 6.4–39.1% Ser [abbreviated as SPG–Ser(6.4)–SPG–Ser(39.1)]. All SPG–Ser samples were soluble in DMSO. In the SPG–Arg series, SPG–Arg(3.6)–SPG–Arg(18.1) were soluble, although the solution of SPG–Arg(18.1) was somewhat cloudy. In SPG–Lys series, on the other hand, SPG–Lys(31.7) was insoluble in DMSO. Thus, subsequent spectroscopic measurements were carried out only for SPG–Lys(6.6), SPG–Lys(12.2), and SPG–Lys(21.2). Presumably, the p*I* of Lys(9.78) is the closest to the medium pH (8.0), so that the SPG–Lys conjugate polymers partially retain the zwitterionic nature although when the degree of the cationic charge is greater than anionic charge, inter-polymeric aggregation is favored, which results in a cloudy solution or precipitate.

Table 1
Molar ratio (%) in the reaction mixtures and introduced percentages (%) of α-amino acid groups (per side-chain glucose unit)

| Molar ratio | Modified SPG | | |
|---|---|---|---|
| $NaIO_4$/side-chain glucose unit | SPG–Arg | SPG–Lys | SPG–Ser |
| 10% | 3.6 ± 0.1% | 6.6 ± 0.3% | 6.4 ± 0.3% |
| 40% | 9.3 ± 0.2% | 12.2 ± 0.2% | 13.2 ± 0.4% |
| 70% | — | 21.2 ± 0.6% | 16.0 ± 1.0% |
| 100% | 18.1 ± 0.3% | — | 28.0 ± 1.5% |
| 500% | 36.0 ± 0.4% | 31.7 ± 0.1% | 39.1 ± 1.2% |

Fig. 2 compares the CD spectra for poly(C), a mixture of s-SPG and poly(C), and a mixture of s-SPG–Arg(3.6) and poly(C). Since neither s-SPG nor s-SPG–Arg(3.6) has any absorbance at the wavelengths presented in Fig. 2, all CD bands can be assigned to conformational changes in the poly(C) chain. It can be seen from Fig. 2 that the spectrum for the s-SPG + poly(C) system is different from that of poly(C) alone in that the 275 nm band increases by 50% and a new band arises near 242 nm [8,9,13]. These spectral changes can be ascribed to complex formation between s-SPG and poly(C), indicating a change into a more ordered helical conformation [8,9,13]. The spectrum of the s-SPG–Arg(3.6) + poly(C) system also has two characteristic bands at 242 and 275 nm. However, the intensity of the CD bands is somewhat weaker. The CD spectra obtained for other SPG–Arg and SPG–Lys samples, when they form the macromolecular complexes with poly(C), were basically similar to that of the SPG–Arg(3.6) + poly(C) system.

In Figs. 3–5, the CD intensity of poly(C) at 275 nm is plotted against temperature. It can be seen from the temperature dependence in Figs. 3 and 4 that the introduction of Arg or Lys enhances $T_m$ values. As shown in Fig. 6, the $T_m$ value tends to increase with the increase in the percentage of α-amino acid introduced. In the SPG–Arg series, the highest $T_m$ value (64 °C) was observed for SPG–Arg(18.1) and in the SPG–Lys series the highest $T_m$ (62 °C) was observed for SPG–Lys(12.2). These values are higher by 13 and 11 °C, respectively, than those of unmodified s-SPG + poly(C) complex (51 °C) [15]. Since the CD spectra of these complexes are basically similar to those of the s-SPG + poly(C) complex (vide supra), one can consider that electrostatic interactions, in addition to hydrogen-bonding and hydrophobic interactions

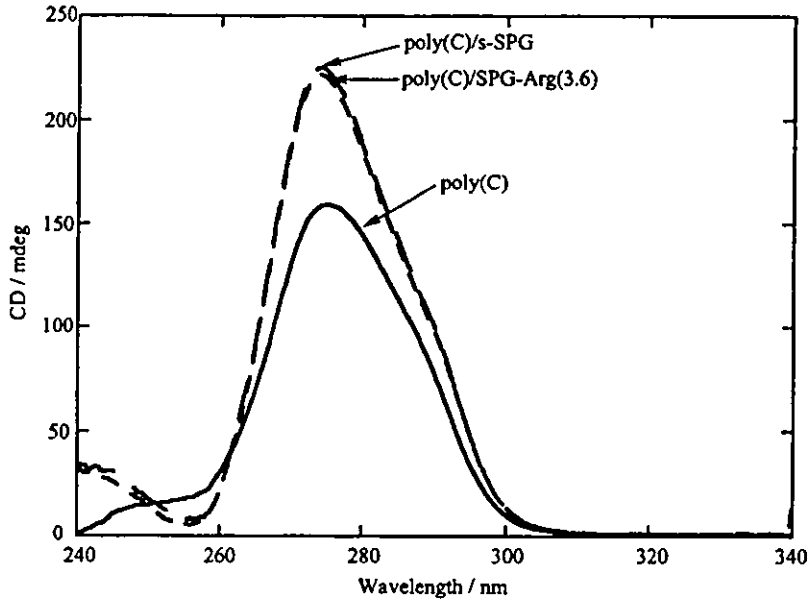


Fig. 2. Comparison of the CD spectra for poly(C), s-SPG + poly(C), and s-SPG–Arg(3.6) + poly(C) measured at 5 °C: [poly(C) (monomer unit)] = $2.5 \times 10^{-4}$ mol dm$^{-3}$ [s-SPG (monomer unit for main-chain)] = $1.9 \times 10^{-3}$ mol dm$^{-3}$, [s-SPG–Arg(3.6) (monomer unit for main-chain)] = $1.9 \times 10^{-3}$ mol dm$^{-3}$, [Tris] = $8.3 \times 10^{-4}$ mol dm$^{-3}$ (pH = 8.0), water:DMSO = 92:8 v/v.

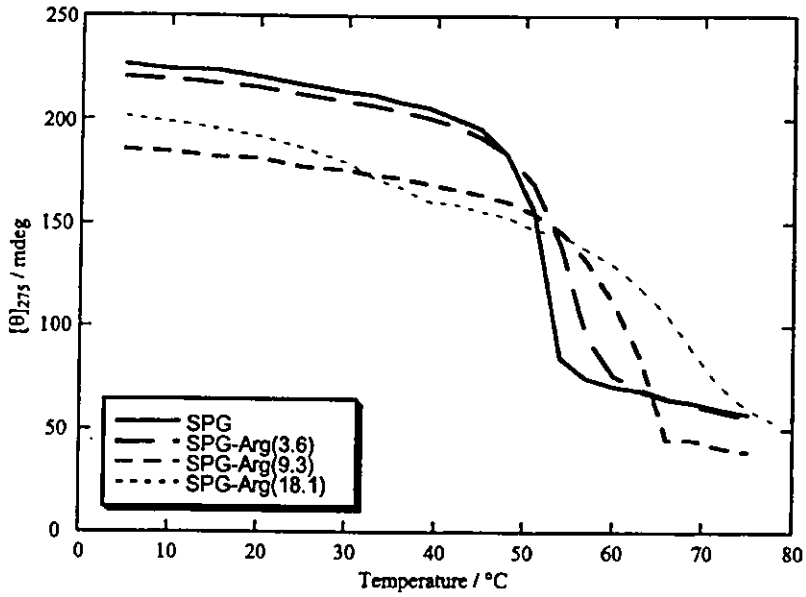


Fig. 3. CD intensity at 275 nm plotted against medium temperature for SPG–Arg + poly(C) systems.

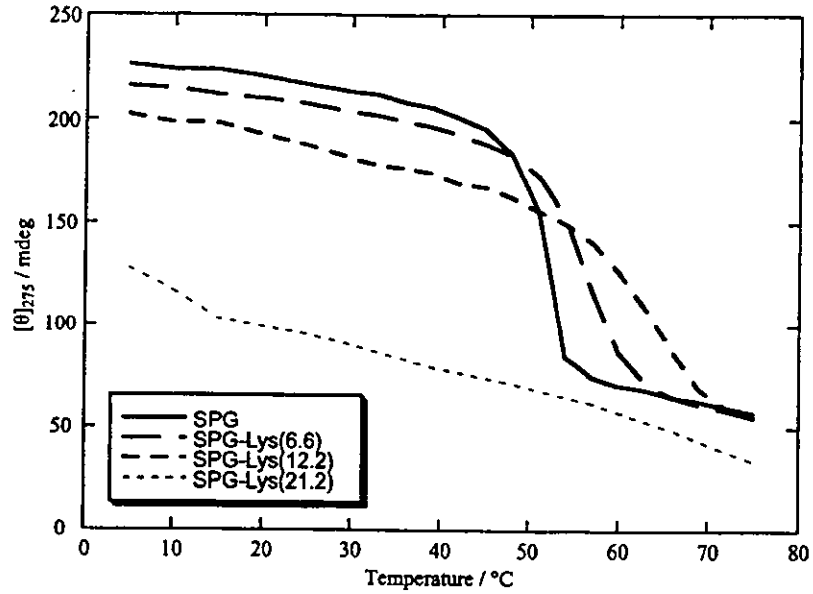


Fig. 4. CD intensity at 275 nm plotted against medium temperature for SPG–Lys + poly(C) systems.

operating in the s-SPG + poly(C) complex, participate effectively in the thermal stabilization of the SPG–Arg and SPG–Lys complexes. As Arg has a guanidinium group capable of acting as a complementary hydrogen-bond donor for a phosphate group, it was expected that the $T_m$ values for the SPG–Arg series might be higher than those for the SPG–Lys series. However, the $T_m$ difference observed in the present system is too small to make this conclusion. Examination of Figs. 3 and 4 also

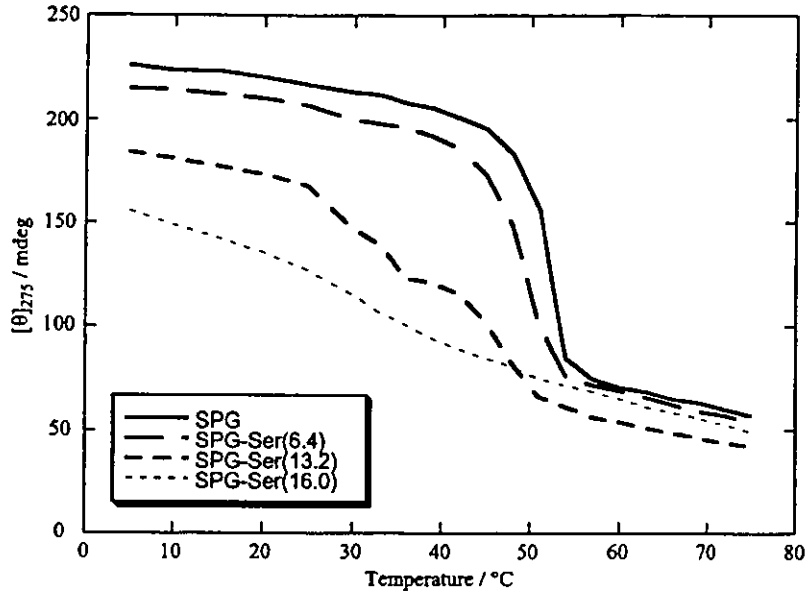


Fig. 5. CD intensity at 275 nm plotted against medium temperature for SPG–Ser + poly(C) systems.

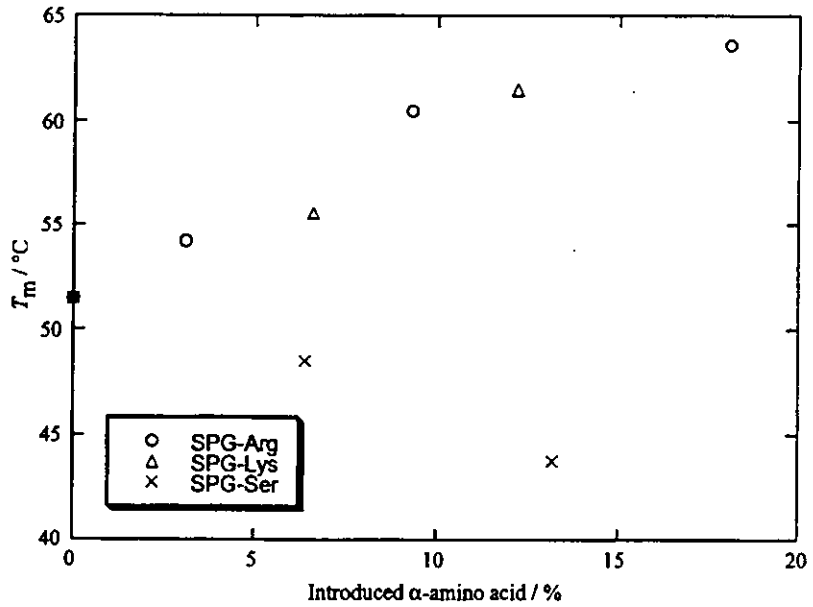


Fig. 6. Plots of α-amino acid percentage introduced (%) vs. $T_m$.

reveals that with the increase in the percentage of α-amino acid introduced, the $[\theta]_{275}$ values in the low temperature region decrease and the degree of cooperativity in the dissociation process (i.e., the gradient of the anti-sigmoidal curvature) decreases. The results imply that the participation of the electrostatic interaction may intensify the thermal stability of the complexes, but may simultaneously induce some disorder in the hydrogen-bonding complementarity between SPG and poly(C). Interestingly, it can be seen from Fig. 4 that in contrast to the high $T_m$ value (62 °C) of the

SPG–Lys(12.2) + poly(C) system, SPG–Lys(21.2) does not interact with poly(C) at all. As mentioned above, SPG–Lys(21.2) is not soluble in DMSO presumably because of the inter-polymeric aggregation caused by the zwitterionic nature. Thus, the nonbinding properties of SPG–Lys(21.2) are also explained by inter-polymeric interaction among SPG–Lys(21.2) polymers occurring in preference to interaction between SPG–Lys(21.2) and poly(C).

On the other hand, Fig. 5 shows that the $T_m$ values for the SPG–Ser series decrease with the increase in percentage of Ser introduced. Since the Ser residue has a $pI = 5.68$ and carries an anionic charge at pH 8, the destabilization is ascribed to the electrostatic repulsion between the like charges in SPG–Ser and poly(C). In fact, complex formation is no longer observed for SPG–Ser(16.0), SPG–Ser(28.0), and SPG–Ser(39.1) even though they are soluble in DMSO and the measurement medium (water:DMSO = 92:8 v/v).

## 4. Concluding remarks

The present paper has demonstrated that the thermal stability of the s-SPG + poly(C) complex can be controlled by the type and the percentage of α-amino acids introduced. The fact that the $T_m$ values can be enhanced above body temperature implies that the present system may be applicable as an artificial vector for an in vivo system. In this context, it is particularly worth emphasizing that the conjugates consist of both nontoxic SPG and α-amino acids. We are now extending this system to the binding of various RNA and DNA species and to their actual transport across biomembranes.

## References

[1] (a) S. Kikumoto, T. Miyajima, S. Yoshizumi, S. Fujimoto, K. Kimura, J. Agr. Chem. Soc. Jpn. 44 (1970) 337–340;
(b) K. Yanaki, W. Ito, W. Kojima, T. Norisuye, N. Takano, H. Fujita, Biophys. Chem. 17 (1983) 337–342.
[2] S. Kikumoto, T. Miyajima, K. Kimura, S. Okubo, N. Komatsu, J. Agr. Chem. Soc. Jpn. 45 (1971) 162–167.
[3] T. Yanaki, T. Norisuye, H. Fujita, Macromolecules 13 (1980) 1462–1466.
[4] T. Norisuye, T. Yanaki, H. Fujita, J. Polym. Sci. Polym. Phys. Ed. 18 (1980) 547–558.
[5] C.T. Chuah, A. Sarko, Y. Deslandes, R.H. Marchessault, Macromolecules 16 (1983) 1375–1382.
[6] T.M. McIntire, D.A. Brant, J. Am. Chem. Soc. 120 (1998) 6909–6919.
[7] B.H. Falch, B.T. Stokke, Carbohydr. Polym. 44 (2001) 113–121.
[8] K. Sakurai, S. Shinkai, J. Am. Chem. Soc. 122 (2000) 4520–4521.
[9] (a) K. Sakurai, M. Mizu, S. Shinkai, Biomacromolecules 2 (2001) 641–650;
(b) K. Koumoto, T. Kimura, K. Sakurai, S. Shinkai, Bioorg. Chem. 29 (2001) 178–185.
[10] T. Kimura, K. Koumoto, K. Sakurai, S. Shinkai, Chem. Lett. (2000) 1242–1243.
[11] K. Sakurai, S. Shinkai, T. Kimura, K. Tabata, K. Koumoto, O. Gronwald, Patent application, PCT, P0524T, 2000.
[12] B.T. Hofreiter, I.A. Wolff, C.L. Mehltretter, J. Am. Chem. Soc. 79 (1957) 6457–6460.
[13] K. Koumoto, T. Kimura, M. Mizu, K. Sakurai, S. Shinkai, Chem. Commun. (2001) 1962–1963.

[14] We cite here the p*I* values of α-amino acids for discussion purposes. Although the p*I* values of N-alkyl derivatives may be somewhat different, the differences are likely small. For example, the p*I* for glycine is 5.97 and that for *N*-methylglycine is 6.10 E.A. Martell, M.R. Smith, Critical Stability Constants, vol. 1, Plenum Press, New York, 1989.

[15] The $T_m$ for the unmodified s-SPG + poly(C) is slightly affected by the media used. For example, the $T_m$ is 49 °C in absence of buffer [13] and 50 °C in $8.3 \times 10^{-4}$ mol dm$^{-3}$ Tris buffer (pH = 8.0) (water:DMSO = 95:5 v/v) [10].

ACADEMIC PRESS

Available online at www.sciencedirect.com

SCIENCE DIRECT®

Bioorganic Chemistry 31 (2003) 216–226

BIOORGANIC CHEMISTRY

www.elsevier.com/locate/bioorg

# Polysaccharide–polynucleotide complexes. Part 7. Hydrogen-ion and salt concentration dependence of complexation between schizophyllan and single-stranded homo RNAs

Kazuo Sakurai,[a,*] Ristuko Iguchi,[b] Masami Mizu,[a] Kazuya Koumoto,[a] and Seiji Shinkai[b]

[a] *Department of Chemical Process and Environments, The University of Kitakyushu, 1-1 Hibikino, Wakamatu-ku, Kitakyushu, Fukuoka 808-0135, Japan*

[b] *Department of Chemistry and Biochemistry, Faculty of Engineering, Graduate School of Engineering, Kyushu University, 6-10-1 Hakozaki, Higashi-ku, Fukuoka 812-8581, Japan*

Received 2 April 2002

**Abstract**

Schizophyllan belongs to a β-1,3-D-glucan family, which exists as a random coil in dimethyl sulfoxide (DMSO) and as a triple helix in water, respectively. The schizophyllan single chain forms a complex with single-stranded homo RNAs in water/DMSO mixed solvents. Using circular dichroism, we studied the complexation and its stability as a function of apparent pH (pH*) in a mixed solvent system and as a function of the salt concentration. The complex is formed in the pH* range 6.5–10, and dissociated in the pH* range 4–6. Both poly(A) and poly(C) adopt a double strand in the pH* range 4–6 and a single strand in the pH* range 6.5–10. Therefore, the conformational change of each polynucleotide is responsible for dissociation/association of the complex, i.e., the single strand of the polynucleotides can form complexes, whereas the double one cannot. This result indicates that hydrogen bonding and similarity of the helix parameters are essential for the complex formation. The melting temperature of the complex reaches the maximum around 0.05 M of NaCl and KCl, and the value of the maximum temperature depends on the cation species.


* Corresponding author. Fax: +81-93-695-3368.
*E-mail address:* sakurai@env.kitakyu-u.ac.jp (K. Sakurai).

0045-2068/03/$ - see front matter © 2003 Elsevier Science (USA). All rights reserved.
doi:10.1016/S0045-2068(03)00034-8

*Keywords:* Schizophyllan; β-1,3-Glucans; Conformational change of polynucleotide; RNA; Polysaccharide–polynucleotide complex

## 1. Introduction

Schizophyllan is a cell wall polysaccharide produced by the fungus *Schizophyllan commune*, where the main chain consists of β-1,3-D-glucans and the one β-(1→6)-D-glucosyl side chain links to the main chain at every three glucose residues [1], as shown in Fig. 1. Yanaki et al. [2] and Young and Jacobs [3] showed that schizophyllan exhibits antitumor activity against *Sarcoma 180* as well as lectin activity against *Limulus amebocyte* lysate. Norisuye et al. [4–7] extensively studied the dilute solution properties of schizophyllan and determined that schizophyllan adopts a triple helix conformation [8] (see (b) in Fig. 1) in water and a random coil in dimethyl sulfoxide (DMSO) [4,5]. In addition, when DMSO is added to the schizophyllan aqueous

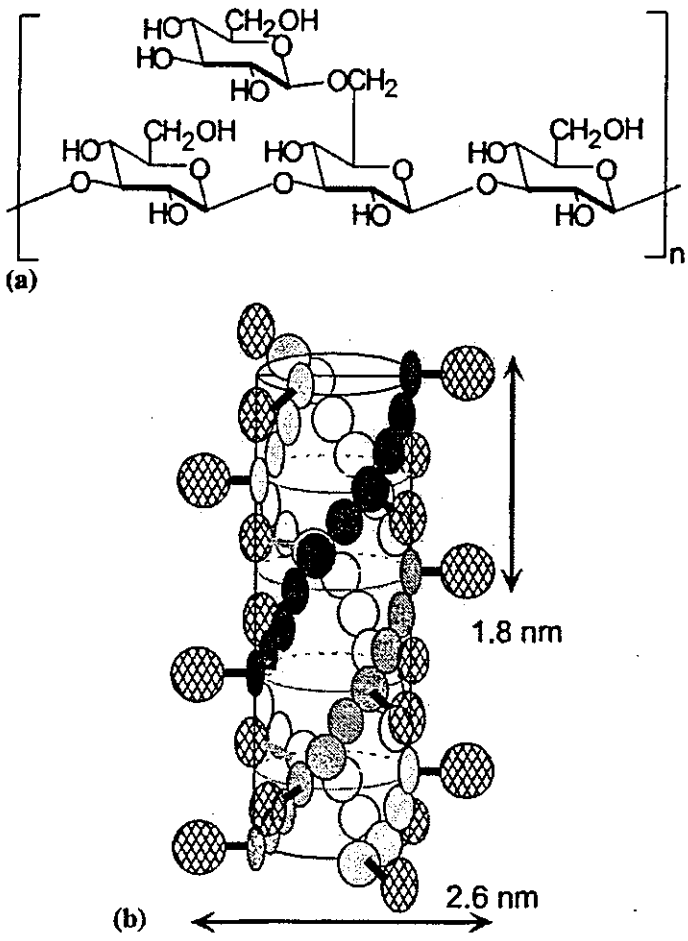


Fig. 1. Repeating unit of schizophyllan (a) and its representative model of the triple-helix (b). In (b), the plain circles represent the main chain glucose residues and the meshed ones, the side chains.

solution (denaturation), the helix remains intact up to the water fraction in the DMSO–water mixture ($V_w$) = 0.14 [5]. However, they found that, when water is added to the DMSO solution (renaturation), the single chain of schizophyllan (s-SPG) collapses at $V_w = 0.14$ owing to hydrophobic interactions [7]. Brant and coworkers [9,10] and Jacobs et al. [11] independently showed that the local structure of the renatured product can return to the original triple helix although the entire structure is not the same as the original rod like molecules. Recently, McCormick et al. [12] found an interesting interaction between schizophyllan and an amphipathic protein called SC3p [12], which plays an important role in fungal attachment to a host organism. These pioneering studies have encouraged efforts to understand the nature of this polysaccharide. The mechanism of its antitumor activity is not well understood at the molecular level and remains a challenging issue in the field of saccharide biochemistry.

Sakurai and Shinkai [13] were the first to demonstrate that s-SPG forms a macromolecular complex with poly(C) and poly(A) during renaturation. This work may provide a new clue to understand the mysterious bioactivity of this polysaccharide. Their subsequent studies [14,15] revealed that (1) two schizophyllan chains and one poly(C) chain form a triple helix and (2) one glucose in each s-SPG, (i.e., two glucose in total) form hydrogen bonds with one cytosine residue (see chemical structure (C) in Fig. 5). Their X-ray crystallography showed that the helix parameters of the complex are close to that of triple-helix schizophyllan: a right-handed $6_1$ triple helix with a 17.4 Å pitch [15]. According to the literature [16], the helix parameter of the single-stranded poly(C) is a right-handed $6_1$ helix with a 18.6 Å pitch. These two parameters are surprisingly close so that we can assume that there should be little loss in the conformational entropy after the complexation. This explains why poly(C) and s-SPG form the complex.[1]

The above discussion indicates that conformational similarity between two chains is important for the complex formation. Polynucleotides also undergo conformational transitions upon changing the hydrogen-ion concentration and the ionic strength [16]. Therefore, complexation presumably depends on these solution properties. In this paper, we explore the relationship between the complexation and the hydrogen-ion and salt concentrations.

## 2. Materials and methods

The triple helix of schizophyllan (t-SPG) was kindly supplied by Taito (Tokyo, Japan). The intrinsic viscosities ([$\eta$]) of t-SPG and s-SPG in water and DMSO at 25 °C were determined to be 6.1 and 0.92 dL $g^{-1}$, respectively, and from those [$\eta$] values the molecular weights were calculated to be $4.5 \times 10^5$ and $1.5 \times 10^5$ (690 and 230

[1] Poly(A) forms a right-handed $9_1$ helix with a 25.4 Å pitch. This parameter is apparently different from that of the complex. However, since the axial rise per residue is close: 2.9 Å for SPG and 3.1 Å for poly(A), we can consider that it is easy for poly(A) to fit the conformation to the complex without major entropy loss.